Available online at www.sciencedirect.com
ScienceDirect
International Journal of Heat and Mass Transfer 50 (2007) 2969–2980
International Journal of HEAT and MASS TRANSFER
www.elsevier.com/locate/ijhmt

Multiscale modeling of particle–solidification front dynamics. Part II: Pushing-engulfment transition

J.W. Garvin, Y. Yang, H.S. Udaykumar *

Department of Mechanical and Industrial Engineering, The University of Iowa, Iowa City, IA 52242, United States

Received 19 February 2006; received in revised form 14 December 2006
Available online 28 March 2007

Abstract

The interaction between a particle and an advancing solidification front is studied using a multi-scale computational model developed in Part I. The flow and temperature fields are solved separately at two disparate scales, i.e. at the overall system scale (''outer region'') and in the thin melt layer (''inner region'') between the particle and the front. The solutions from the inner and outer regions are coupled at a matching region. The coupled dynamics of the particle and phase boundary motion, including lubrication and disjoining pressure effects in the premelted film between the particle and the front is captured in the simulations. Results show that particle pushing (as opposed to particle engulfment) can occur when the ratio of thermal conductivity of the particle to the melt, $k_p/k_l < 1$. The velocity of the solidification front at which the transition from particle pushing to particle engulfment occurs, i.e. the critical velocity for particle engulfment, is naturally obtained from the coupled dynamics. No ad hoc assumptions to identify the critical velocity need be made. The results also provide insights into the physics of particle–solidification front interactions.

1. Introduction

When a particle is approached by an advancing solidification front, the latter must obtain a certain ''critical velocity'' in order to engulf the particle [1]. If the solidification velocity is below this critical value, the particle will be pushed, and if the front velocity is above this value, the particle will be engulfed. The overall transport phenomena and the forces resulting in particle pushing/engulfment by a solidification front are multiscale in nature. This is due to the importance of the dynamics of the thin liquid film between the particle and front in determining the fate of the particle. In Part I a general methodology was presented for solving this multiscale problem, where flow solutions in the ''inner'' (melt film) region and the ''outer'' (overall front-particle system) region were obtained and coupled at a ''matching'' region. This paper will employ the technique presented in Part I to compute the front-particle interaction dynamics and to shed light on the physics underlying particle pushing/engulfment.

1.1. Role of thermal and fluid transport in the ''outer'' region

In Part I (Fig. 1), the overall view of the problem is given. A solidification front traveling upward with velocity v_s approaches the particle until it is a small distance d from the particle. As a solidification front approaches the particle to this small (nanometer-scale) separation repulsive disjoining pressures (and a resultant force on the surface of the particle F_I) in the intervening melt film become large and will set the particle in motion away from the front. To replenish the melt in the gap between the particle and the front a net flux of melt into the gap is required. The melt layer therefore acts as a lubrication film, resulting in a large drag force (F_D) that acts to push the particle back towards the solidification front. The particle begins to move upward at a velocity v_p. The fluid dynamics and thermal transport play a major role at the microscale (overall domain) and the intermolecular forces and heat and mass

* Corresponding author. Tel.: +1 319 384 0832; fax: +1 319 335 5669.
E-mail address: ush@icaen.uiowa.edu (H.S. Udaykumar).

0017-9310/$ - see front matter © 2007 Elsevier Ltd. All rights reserved.
doi:10.1016/j.ijheatmasstransfer.2006.12.022

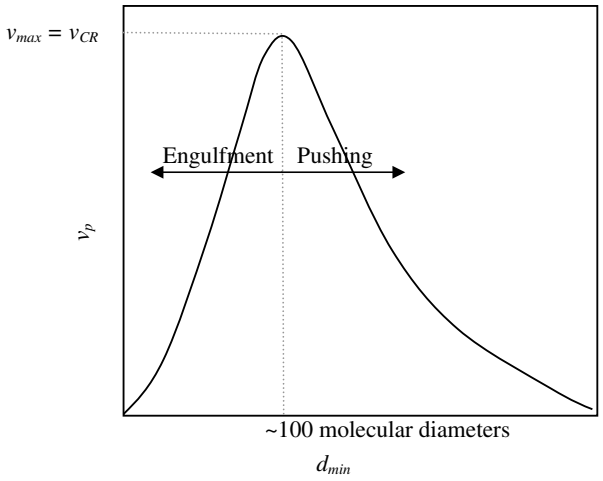

Fig. 1. Illustration of how the critical velocity is determined in [6].

transport compete in the melt layer sandwiched between the particle and the front. The overall solidification front morphology is governed by both scales as its shape changes due to the thermal conduction phenomena and material properties (particularly the ratio of particle to melt thermal conductivities k_p/k_l) as well as mass and thermal transport in the melt layer. Thus, the challenge in simulating solidification front interactions with particles is to capture this coupling between the outer (overall particle–front system) and inner (premelted layer) scales. In this paper, a multiscale model described in Part I is applied in the present paper to study front–particle interactions.

1.2. Physics of flow and interaction forces in the "inner" region

When a solidification-front approaches it, a particle will experience intermolecular forces acting across the intervening melt gap that tends to push it away from or pull it towards the solidifying interface. These long-range (dispersive) intermolecular forces are not significant until the interfaces become sufficiently close to each other (order of nanometers). In a continuum representation, these forces are the result of a disjoining pressure in the melt film [2]:

$$\Pi = \frac{A}{6\pi d^3}, \tag{1}$$

where Π is the disjoining pressure, A is the Hamaker constant and d is the distance between the two surfaces. The disjoining pressure is defined such that a negative Hamaker constant results in a repulsive force between the two interfaces whereas a positive Hamaker constant results in an attractive force between the interfaces. The value (and sign) of the Hamaker constant depends on the system in question, typical values being $\pm 10^{-19}$ J.

The Hamaker constant, and hence the disjoining pressure, can also be related to the surface free energies of each of the phases involved [3,4]:

$$A = -4\pi d_0^2 \Delta\gamma, \tag{2}$$

where

$$\Delta\gamma = \gamma_{sp} - \gamma_{lp} - \gamma_{sl}, \tag{3}$$

where γ_{sp} is the free energy of the solid (solidification front)–particle interface, γ_{lp} is the liquid–particle interfacial free energy and γ_{sl} is the solid–liquid interfacial free energy. The d_0 is a constant with the dimensions of length and has a typical value of several molecular diameters [3,4].

Note that in systems where $\Delta\gamma$ is positive, as the solidification front gets close enough to the particle a repulsive disjoining pressure forms to push the particle away as it is more energetically favorable for a layer of liquid to exist between them. The opposite is true when the interfacial free energy difference is negative, i.e. the solidification front is attracted to the particle.

Due to the existence of a disjoining pressure a change in the melting temperature of the interacting interfaces will result through the Clausius–Clapeyron relation [5]. If $\Delta\gamma > 0$, a layer of liquid will exist between the solidification front and the particle even when the temperature is lower than that of the bulk melting temperature of the solidifying medium. This depression of the equilibrium melting point leads to a premelted film between the two solid surfaces. The solid–liquid interface temperature in the presence of such a premelted film is given by

$$T_i = T_m - \left(\frac{\lambda}{d}\right)^3 T_m, \tag{4}$$

where λ is an interaction length scale [6].

The existence of a premelted film and the interfacial temperature depression can have a significant effect on front-particle interaction. There have been several theoretical studies where the premelting effect was not taken into account when studying particle–solidification front interactions [1,7–11]. When the premelting effect is neglected, the solidification front can, theoretically, approach the particle all the way down to a zero gap thickness [7–10]. Finding the critical velocity for such a case would then rely on adopting a cut-off value for the minimum value for the gap thickness d (typically 7 molecular diameters) before engulfment is declared [7–10]. Other studies have included the effect of the premelted layer [6,12,13] on the particle–solidification front system [6]. In [6] for instance, for steady-state pushing of a particle by a front, a variation of the particle velocity (v_p) versus the minimum gap thickness for steady pushing (d_{min}) is obtained, as illustrated in Fig. 1. A linear stability analysis of the steady pushing solutions was performed and it was suggested that the maximum velocity in Fig. 1 is the critical velocity (v_{CR}). Small perturbations of the system to the left of this maximum in the $v_p - d_{min}$ curve will result in engulfment whereas to the right of the maximum the steady pushing mode is maintained. The d_{min} corresponding to the identified critical velocity is of order of 100 molecular diameters (or tens of nanometers) in contrast to the Angstrom thick cutoff

adopted in the aforementioned studies [7,8,14] where premelting effects were not included. In the current study, the results for the particle–solidification front interaction with premelting effects will be compared to those without premelting (i.e. when $T_i = T_m$) and an alternative explanation for the critical velocity will be presented.

2. Simulation of particle–front interaction

In order to study the particle–solidification front interactions, the directional solidification setup is used for the phase boundary calculations. The values of the variables/parameters used in this work are given in Table 1. As described in Part I, the particle is initially placed in the center of the computational domain and the solidification boundary is placed some distance below it. A mesh size of 202×322, with a 202×160 grid points used in the region corresponding to the region $3.0 \leqslant y^* \leqslant 7.0$, i.e. where the particle and front initially lie and where the interaction occurs, was used for the current simulations. This mesh size was determined to yield grid independent results in Part I. To obtain suitable initial conditions, the system is first brought to steady-state by solving the heat conduction equation for an extended time before the phase boundary is allowed to move. After the steady-state temperature values are reached, the phase boundary is allowed to move towards the particle and the subsequent interaction is simulated using the coupled multiscale model.

The main effects that are studied in the cases presented in the following are:

1. The effect of the depression in interface temperature caused by the disjoining pressure in the premelted layer (inner region). In particular we seek to understand: (a) the effect of the depression of interface temperature on pushing/engulfment of the particle and (b) the additional physics that premelting brings into the problem, particularly as it relates to identification of critical velocity.
2. The effect of thermal conductivities of the particle and melt on the evolution of the phase boundary and its coupling with the dynamics of the premelted layer. In particular, what effects do the thermal conductivities have on predictions of critical velocity for engulfment?

2.1. Results

2.1.1. Effects of interface temperature depression due to premelting

When the thermal conductivity of the particle is the same as that of the melt (i.e. $k_p/k_l = 1$), the solidification front remains planar as it approaches the particle. Fig. 2 shows the evolution of the interfaces as well as the temperature/pressure contours for a solidification front moving upward at a speed (v_s) of 100 μm/s toward a particle of 1 μm diameter. In the absence of a premelting-induced depression of temperature (i.e. when $\lambda = 0.0$) the solidification front remains flat as it approaches the particle and follows the equilibrium melting point isotherm. Fig. 2(a) and (b) show the isotherms and outer region flowfield (pressure contours and streamlines) at an instant of time when the front is just beginning to approach the particle. Fig. 2(c) and (d) show the isotherms and outer region flowfield at a time when the particle is being steadily pushed by the front. As a contrast, Fig. 3 illustrates the effects of a premelted layer on a planar (i.e. $k_p/k_l = 1$) solidification front moving towards a particle. In fact, when $k_p/k_l = 1.0$, the only factor that changes the solidification front shape is the depression of the interface temperature due to the premelting effect. This effect begins to manifest only when the front and particle approach close enough that intermolecular forces begin to act between the surfaces, i.e. interface planarity is maintained until such time. As seen from Fig. 3, after the premelting effect sets in, the solidification front (indicated by the bold line in Fig. 3) does not lie on the melting temperature isotherm in the region beneath the particle. Apart from altering the thermal field in the melt film between the particle and the front, the premelting effect has a critical impact on the dynamics of the particle–front interaction. As shown in Fig. 3, in contrast to the case where the temperature depression due to premelting was not included in the simulations (see Fig. 2), the particle

Table 1
Values of the constants/material properties used in calculations (the values for the material properties were adopted from [8])

Constant/material properties	Definition	Value used in present calculations
μ	Dynamic viscosity of melt	0.003 Pa s
ρ	Density of melt	2365 kg/m^3
R_p	Particle radius	10^{-6} m
G_L	Temperature gradient in the melt	10^4 K
A	Hamaker constant	-8.0×10^{-19} J
λ	Interaction length used in premelting expression	2.0×10^{-10} m
k_l	Thermal conductivity of the melt	100 W/mK
k_s	Thermal conductivity of the solid	100 W/mK
k_p	Thermal conductivity of the particle	1–100 W/mK
α_l	Thermal diffusivity of the melt	5.15×10^{-5} m^2/s
T_m	Bulk melting temperature of the melt	933 K
H_{sl}	Latent heat of fusion per unit mass	399 000 J/kg

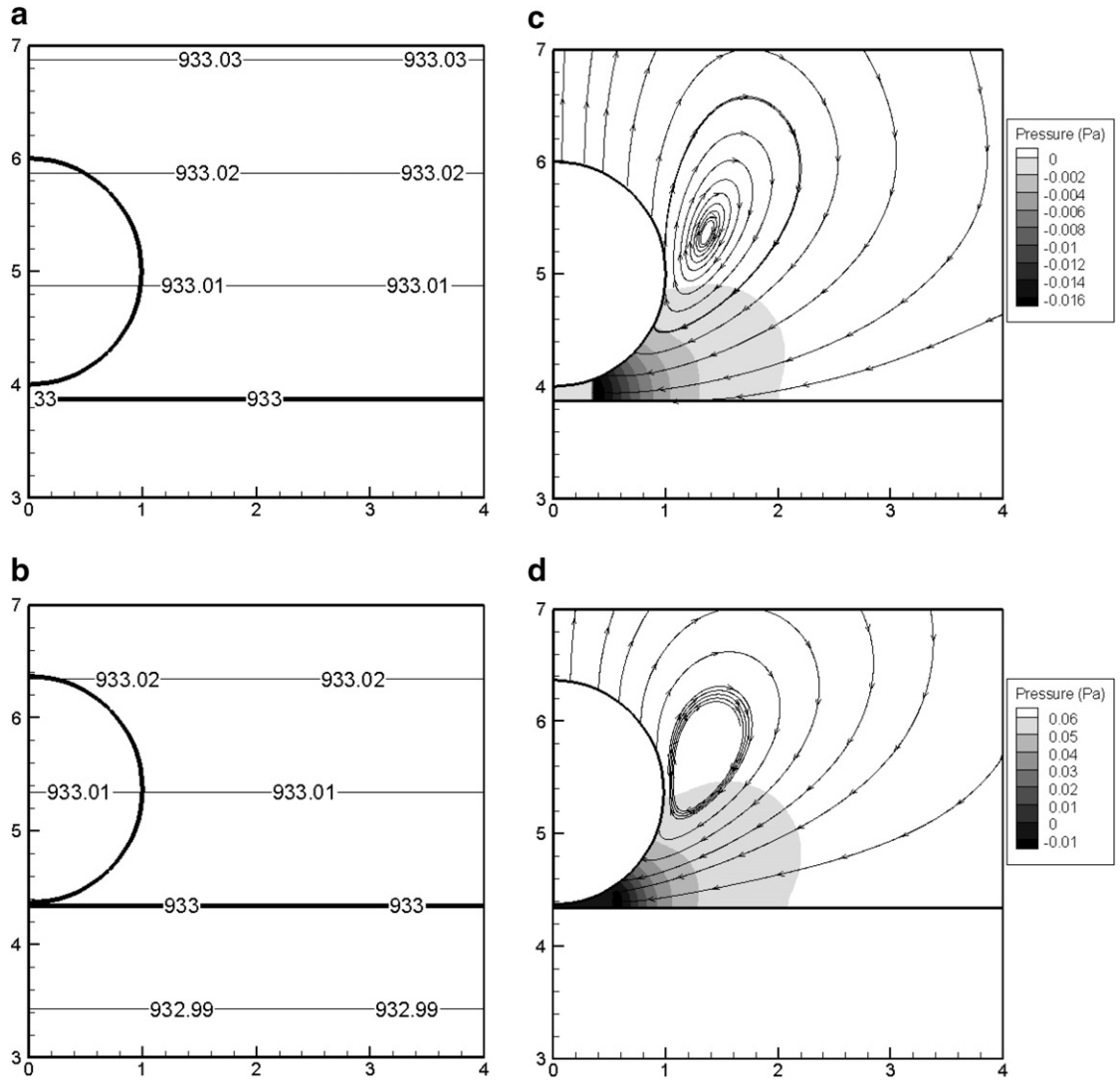

Fig. 2. Results for a system where the solidification velocity is 100 μm/s with no premelting ($\lambda = 0$), $k_p/k_l = 1.0$ and $R_p = 1$ μm. (a) and (b) temperature fields at two time instants during the interaction of the front and the particle. (a) is early in the interaction and (b) is later in the interaction. (c) and (d) the pressure field corresponding to the instants shown in (a) and (b).

in this case is engulfed by the front. Clearly, inclusion of the premelting effects leads to a drastically different outcome in particle–front interactions when compared to the case without premelting effects. Insight into the physics behind the different consequences of the front-particle interactions in Figs. 2 and 3 are obtained by examining the dynamics of the particle, as explained below.

Fig. 4 shows the details of the dynamics of the particle and the front for the case corresponding to Fig. 2, i.e. when the depression of temperature due to premelting is neglected. Fig. 4(a) and (b) show velocity versus time and d_{min} versus time curves respectively. The velocity versus time curves indicate the variation with time of the particle velocity (v_p), the solidification front velocity far from the particle v_s and the tip/trough velocity v_t of the front (i.e. the front velocity right underneath the particle on the symmetry line). At the start of the simulation, $v_t = v_s$; the solidification front is flat and continues to remain flat until it approaches the particle. Due to the disjoining pressure as the gap between the particle and the front narrows (Fig. 4(b)), the particle then begins to accelerate until its velocity matches that of the solidification and tip velocity (i.e. $v_p = v_s = v_t$), at which point a steady pushing mode is reached. Fig. 4(b) illustrates the variation of the minimum distance (d_{min}) between the particle and the solidification front versus time. The d_{min} eventually goes to a steady value at around 20 nm and maintains a steady value; hence a pushing mode is reached. The plot of the forces acting on the particle, shown in Fig. 4(c) is illustrative. As seen in the figure, the repulsive intermolecular force and the opposing drag force increase in magnitude as the front starts to interact with the particle. Initially, the repulsive intermolecular force provides an impulse to the particle. Due to the small inertia of the system, the opposing drag force is set up immediately and the total resulting force falls to a small value, as seen in Fig. 4(d). The repulsion of the particle

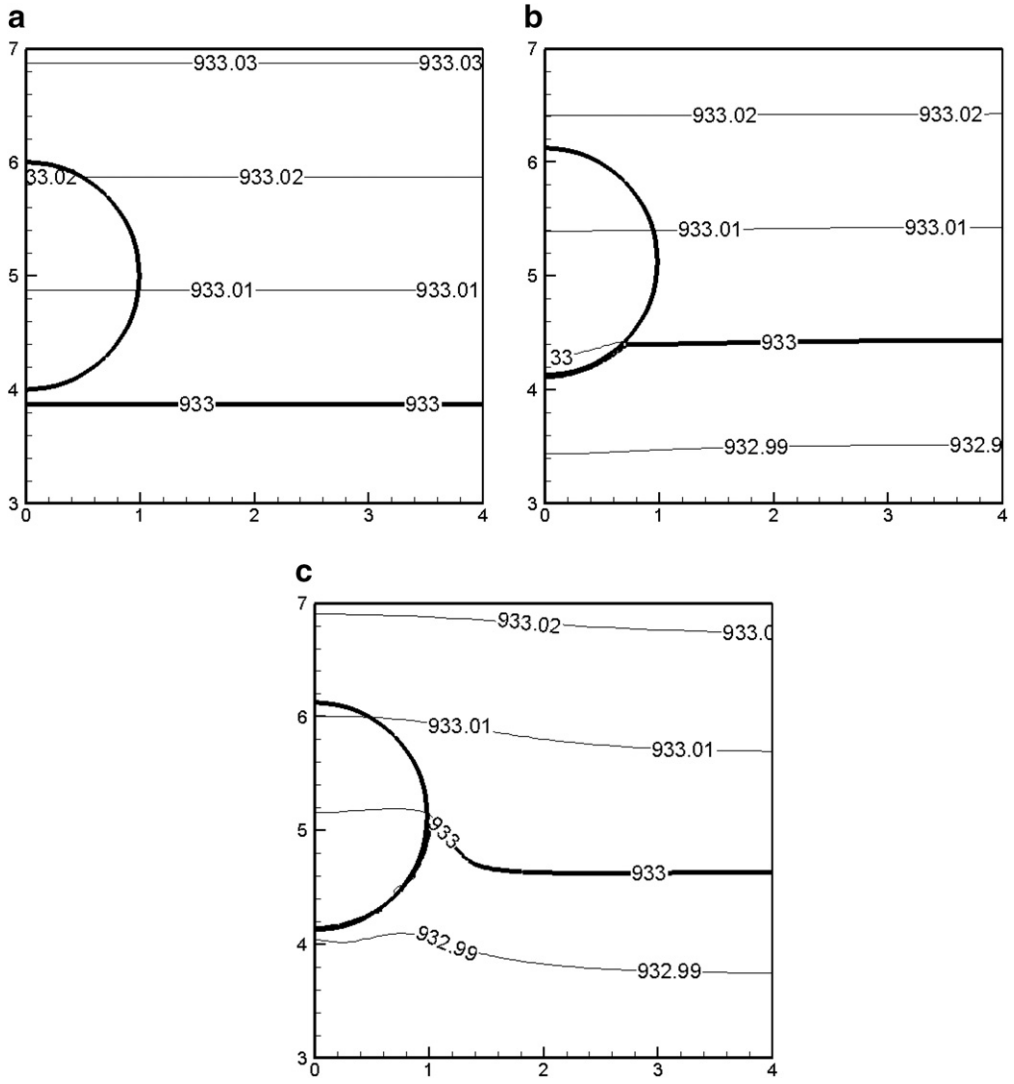

Fig. 3. Temperature contours of a system where the solidification velocity is 100 μm/s, with premelting included ($\lambda = 2 \times 10^{-10}$ m), $k_p/k_l = 1.0$ and $R_p = 1$ μm. (a)–(c) show the contours and the interfaces (thick lines) at three instants in the interaction sequentially from early to later time.

and its motion away from the front also sets up the lubrication flow in the melt layer yielding the viscous pressure losses suffered by the incoming flow of melt from the outer region. The difference between the forces remains small during the interaction, indicating the subtle nature of the front-particle interaction. At the steady pushing condition, which is quickly reached in this case, the forces are nearly in balance, although there is a slight oscillatory tendency around the steady-state.

Fig. 5 shows the details of the dynamics in the situation corresponding to Fig. 3, i.e. where the premelting effect on the melting temperature is included. Clearly the consequences vis-à-vis the dynamics of the particle are entirely different from that shown in Fig. 4. Here, the particle velocity first increases under the influence of the repulsive intermolecular force (Fig. 5(c)), and the resultant force behavior (Fig. 5(d)) is quite similar in the initial stages to the case shown in Fig. 4. Therefore, at least initially, there is little difference caused by the melting point depression due to premelting. However, note that due to melting point depression caused by the disjoining pressure in the premelted film, the solid–liquid interface velocity under the particle continually decreases with respect to that of the particle, as shown in Fig. 5(a). This leads to the formation of a trough under the particle as shown in Fig. 3, in contrast to the nearly planar interface in Fig. 2. The consequence of this trough formation is that the opposing drag force is enhanced and therefore the resultant force becomes negative, i.e. it is directed towards the particle. Consequently, the particle velocity also drops off, as shown in Fig. 5(a). Meanwhile, away from the particle the solid–liquid interface continues to travel at the velocity ($v_s > v_p$). Thus, as shown in the sequence in Fig. 3(a)–(c), the particle is quite rapidly engulfed by the front. The subtlety of the non-equilibrium behavior of the particle–front system is evident from these two cases. Note that, as shown in the isotherm plots in Figs. 2 and 3, the differences in the temperature fields between the two cases are modest. The

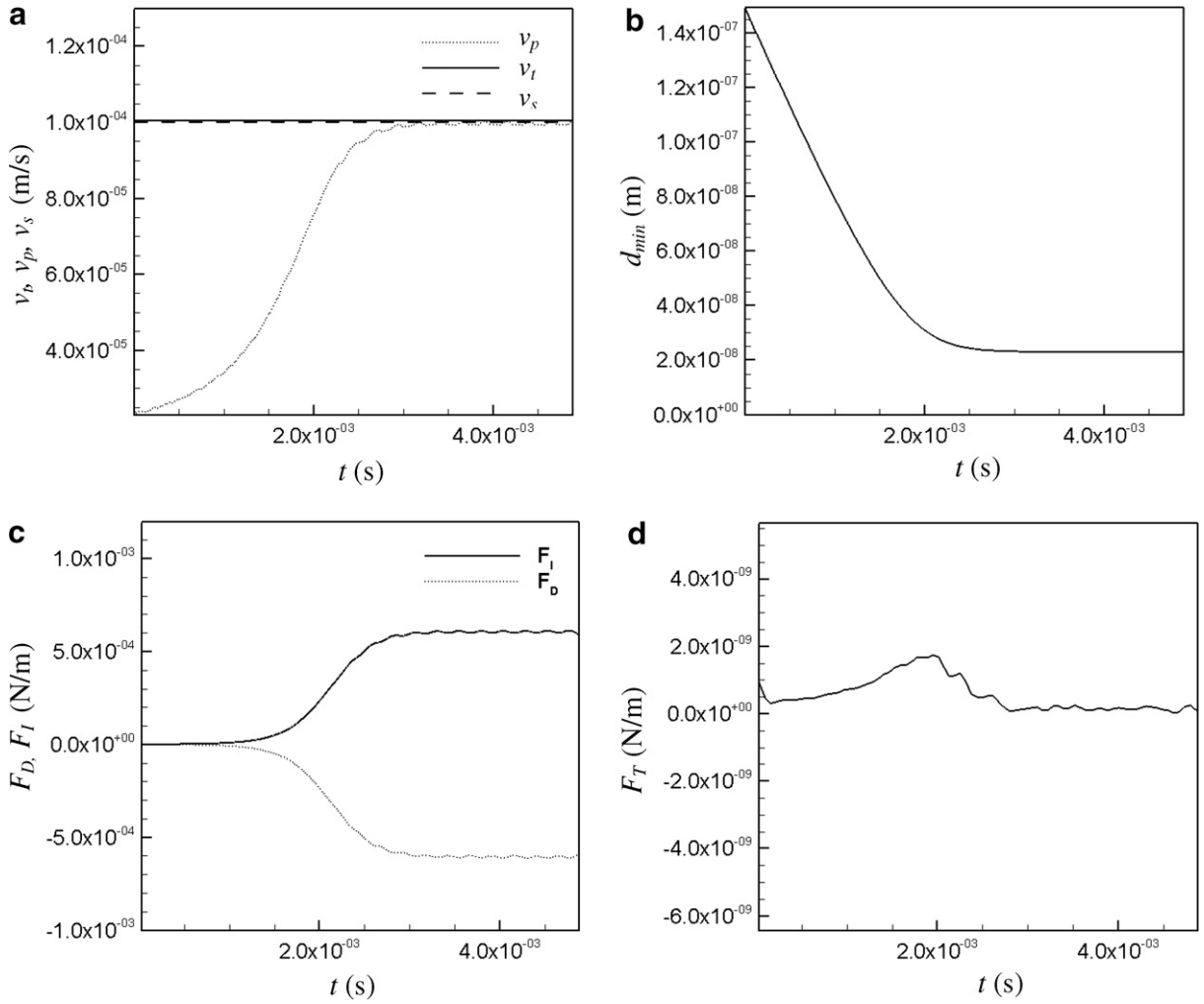

Fig. 4. Behavior of the particle for the case of solidification = 100 μm/s. There is no premelting ($\lambda = 0.0$ m) , $k_p/k_l = 1.0$ and $R_p = 1$ μm. (a) Velocity versus time, the velocities of the particle (v_p), tip of the solidification front (v_t is the velocity of the front right under the particle) and the flat front away from the particle (v_s) are indicated in the figure. (b) d_{min} versus time, (c) the repulsive intermolecular force (F_I) and the drag force (F_D) versus time and (d) the total force (F_T) versus time.

consequences for the front-particle interaction however are decisive. It is worthwhile to note here that these subtle effects are captured by the present multiscale model.

2.1.2. Effects of thermal conductivity of particle relative to melt – determination of critical velocity for engulfment

As indicated by the above results, a critical factor in determining whether a particle will be pushed or engulfed by a solidifying interface is the shape (particularly convexity/concavity) of the solidification front. The ratio of thermal conductivity of the particle to that of the melt (k_p/k_l) plays a major role in determining the solidification front shape [7,9,10,15–18]. If $k_p/k_l < 1.0$, heat transfer through the particle is impeded, causing the isotherms to orient themselves such that a convex protuberance is formed underneath the particle. On the other hand, if $k_p/k_l > 1.0$, heat flows into the particle more readily and causes the isotherms to orient themselves such that the front assumes a concave shape under the particle.

The computational setup used to demonstrate the effect of the thermal conductivity ratio is the same as that used in the previous cases. The value of $k_p/k_l = 0.01$ (corresponding to typical metal-matrix composites) is chosen and the particle radius is 1 μm. The premelting effect is included in all cases. The values of the parameters employed are given in Table 1. The first case studied is one where the solidification velocity is 245 μm/s. The evolution of the temperature contours (with the interfaces shown as bold lines) is shown in Fig. 6. The solidification front is started farther away from the particle than in the $k_p/k_l = 1.0$ cases. This increased distance ensures that the tip velocity reaches a steady value (with a steady convex protuberance under the particle) before it interacts with the particle (Fig. 6(a)). When the interface approaches the particle and the premelting and disjoining pressure effects act in the inner region (gap) between the front and the particle in the present multiscale model, the convex interface in the present case begins to flatten (Fig. 6(b)). As shown in

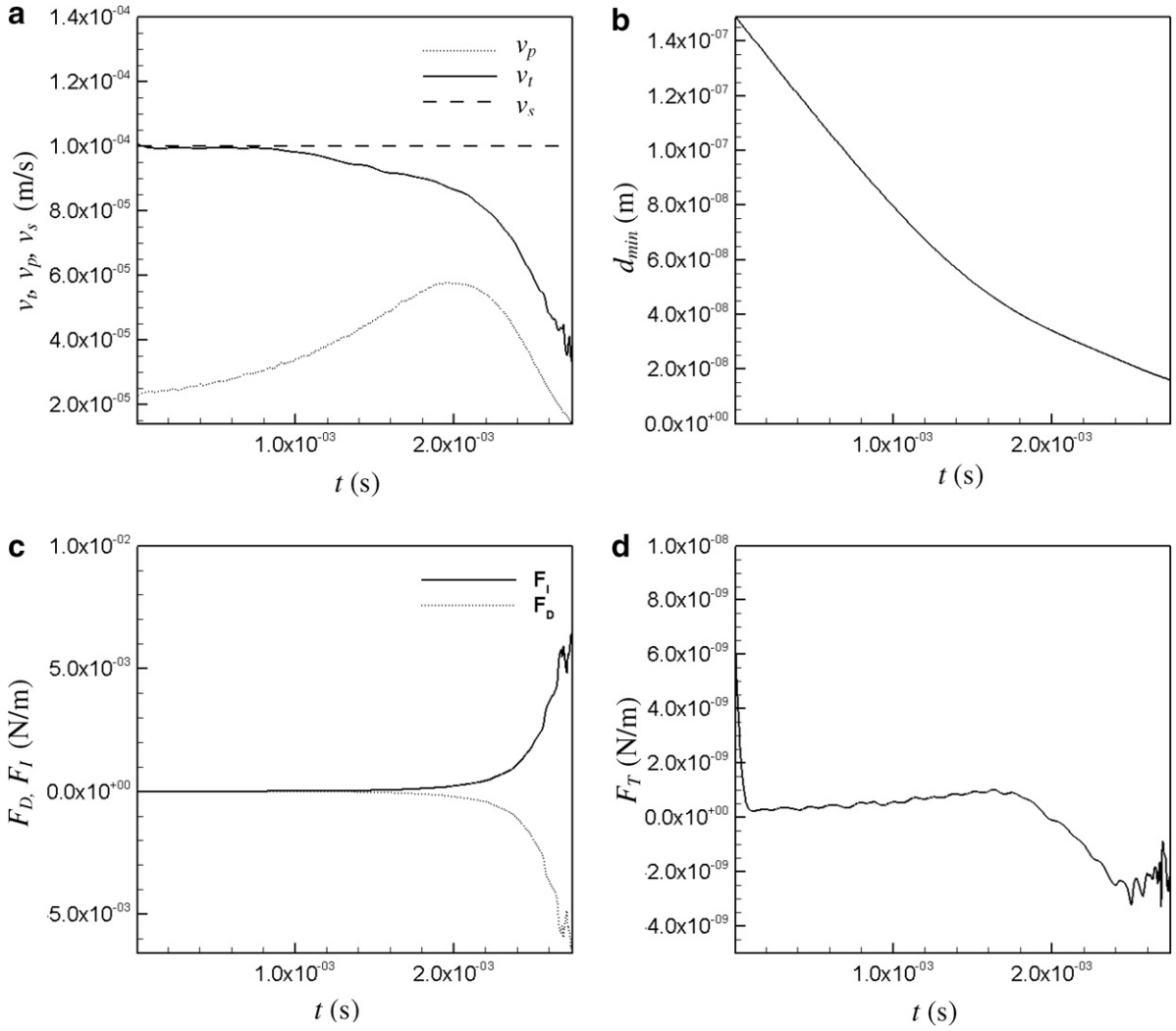

Fig. 5. Behavior of the particle for solidification velocity = 100 μm/s, $\lambda = 2 \times 10^{-10}$ m (premelting included) , $k_p/k_l = 1.0$, $R_p = 1$ μm. (a) Velocity versus time, the velocities of the particle (v_p), tip of the solidification front (v_t is the velocity of the front right under the particle) and the flat front away from the particle (v_s) are indicated in the figure. (b) d_{min} versus time, (c) repulsive intermolecular force (F_I) and the drag force (F_D) versus time and (d) the total force (F_T) versus time.

Fig. 6(c) eventually the interface assumes a concave shape under the particle and the particle is engulfed by the front. The dynamics of the interaction is illustrated in Fig. 7. Fig. 7(a) shows that prior to contact the solidification velocity directly below the particle (v_t) is greater than that far away from it (v_s). The particle velocity initially rises due to the predominance of the repulsive intermolecular forces. Initially the drag force is weaker than the intermolecular force as the interface is convex and the lateral extent of the lubrication layer is small. Eventually, however, the opposing drag force strengthens, particularly as the interface below the particle assumes a concave shape (Fig. 6(c)). Thereafter, both the particle velocity as well as the tip velocity v_t fall to values less than v_s. This results in the eventual engulfment of the particle.

When the solidification velocity is decreased to 230 μm/s very different results are obtained. Fig. 8 shows the interface evolution and the pressure contour maps for this case. Clearly, here the particle is pushed along steadily ahead of the convex solidification front and the outer pressure field settles to a steady-state. From the corresponding velocity versus time plot and the d_{min} versus time plot in Fig. 9 it is clear that the particle is indeed pushed by the front. In contrast with the previous case, the particle velocity in this case rises past the tip velocity and then begins to settles down to the front velocity v_s. The rise in the particle velocity is due to the disjoining pressure force outweighing the drag force right at the beginning of the interaction. However, once the particle velocity increases significantly, the drag force rises. This restores the forces into a nearly balanced condition until eventually the particle velocity, and the tip velocity, oscillate slightly around the pull/solidification velocity. The final minimum gap thickness at which quasi-equilibrium is established is quite significant (~180 nm). The previous two cases indicate that there is a boundary between the solidification velocities of 230

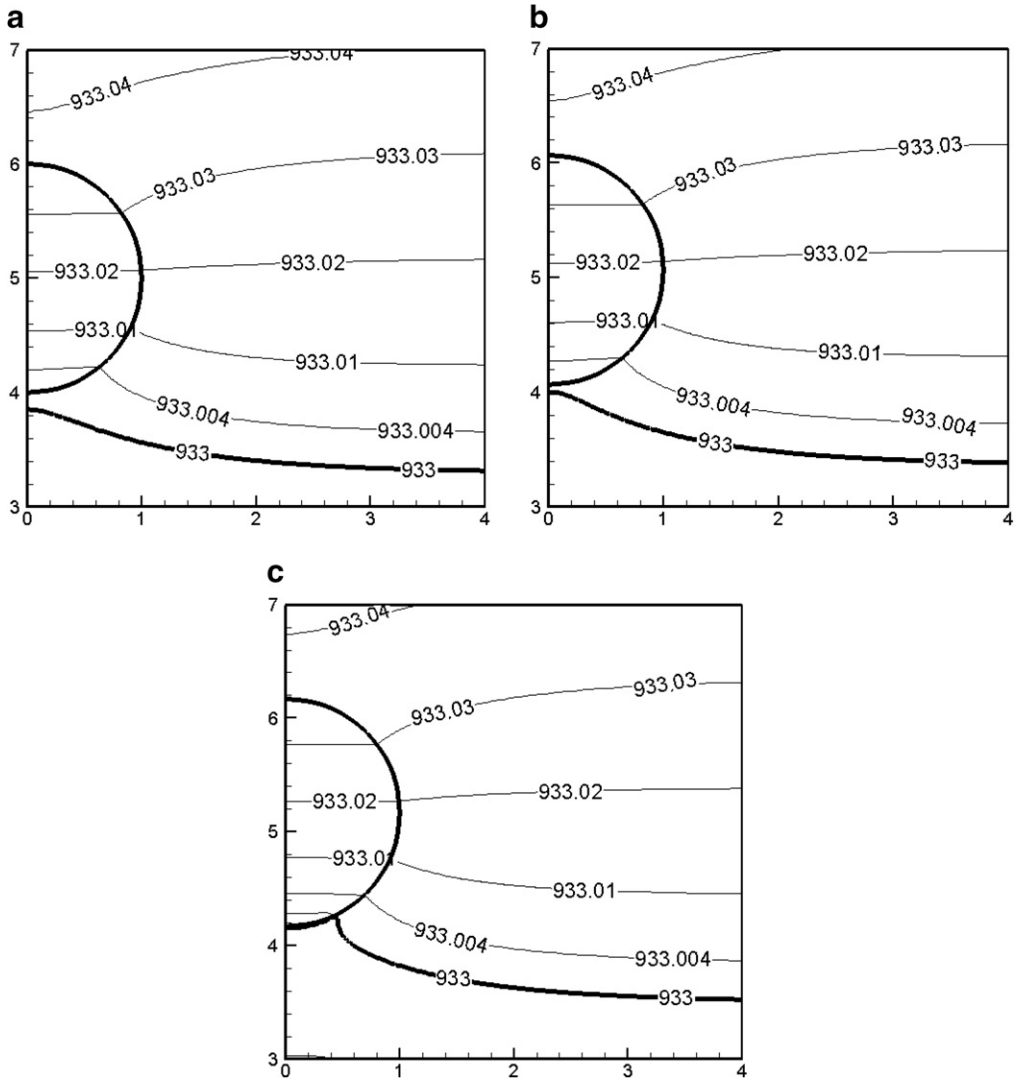

Fig. 6. Temperature contours of a system where the solidification velocity is 245 μm/s, with premelting included ($\lambda = 2 \times 10^{-10}$ m), $k_p/k_l = 0.01$ and $R_p = 1$ μm. The interfaces are shown in bold lines. (a)–(c) are sequentially arranged in increasing time as the interaction proceeds. In (c) the solid–liquid interface has made contact with the particle and is beginning to engulf it.

and 245 μm/s that demarcates the pushing and engulfment regimes. Identification of this boundary will yield the critical velocity for the parameters chosen above.

To identify critical velocities for pushing-engulfment transition, a series of studies were performed by choosing different solidification velocities in the range of 100–500 μm/s. To examine the behavior over this range of solidification velocities, instead of plotting the behavior of v_p against time and d_{min} against time separately, it proves to be more instructive to plot v_p against d_{min} as they evolve in time in each case. These are essentially phase–space plots of the evolution of the particle–front dynamical system. Fig. 10(a) shows the phase–space plot for the $k_p/k_l = 1.0$ cases, including the one that was studied earlier. Note that the arrowheads on the trajectories in phase space show the progression in time. Interestingly, the shape of the curves are similar to the shape of the plots that Rempel and Worster [6] obtained in their steady-state predictions of particle–solidification front interactions. In their work, however, the curve is obtained for a steady-state particle velocity versus a steady-state d_{min} when the particle and front are in a steady pushing interaction. Since their analysis does not cover the full unsteady interaction between the front and the particle, they demarcate the critical velocity using linear stability of the steady-state solutions, i.e. that the steady-state is stable only to the right of the maximum in the curve illustrated in Fig. 1 (hence a pushing regime exists), while it is unstable to the left of the maximum (and engulfment results). Therefore the velocity corresponding to the maximum in the curve is the critical velocity in their analysis. In the current work it is the evolution of the particle velocity and the d_{min} that is being plotted in the phase–plane plot, not the steady-state pushing relationship between v_p and d_{min}.

Using the present multiscale analysis, it is found that the $k_p/k_l = 1.0$ system will always experience engulfment. In

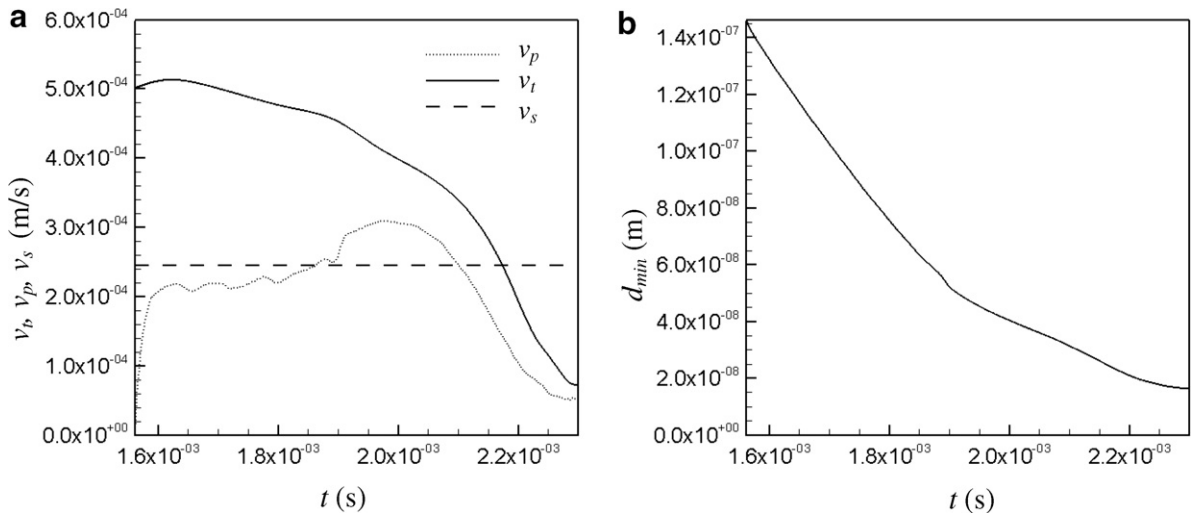

Fig. 7. Behavior of the particle for solidification velocity = 245 μm/s, $\lambda = 2 \times 10^{-10}$ m (premelting included), $k_p/k_l = 0.01$, $R_p = 1$ μm. (a) Velocity versus time, (b) d_{min} versus time.

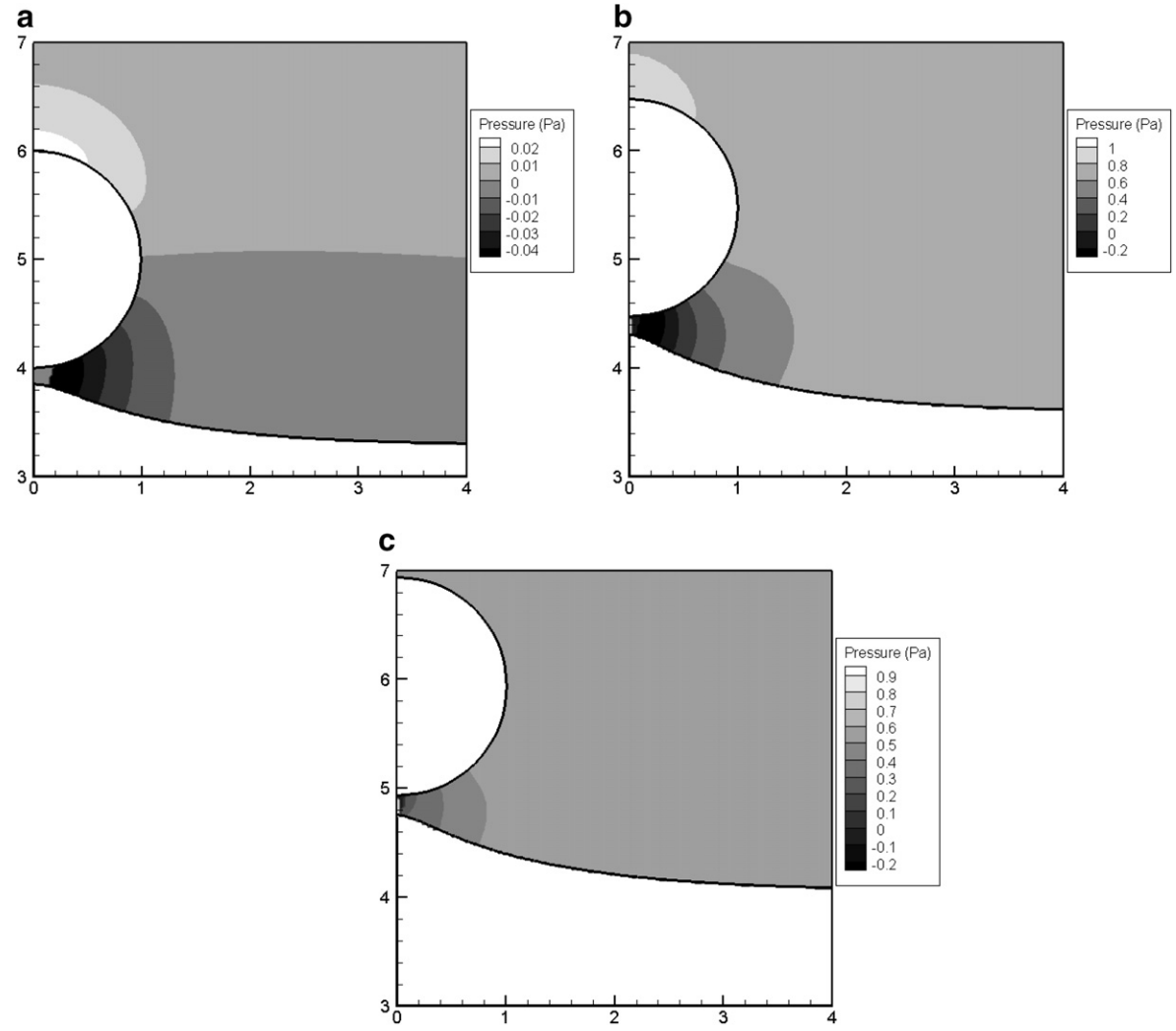

Fig. 8. Pressure contours of a system where the solidification velocity is 230 μm/s, with premelting included ($\lambda = 2 \times 10^{-10}$ m), $k_p/k_l = 0.01$ and $R_p = 1$ μm. (a)–(c) show the contours in increasing sequence of time as the front approaches and interacts with the particle.

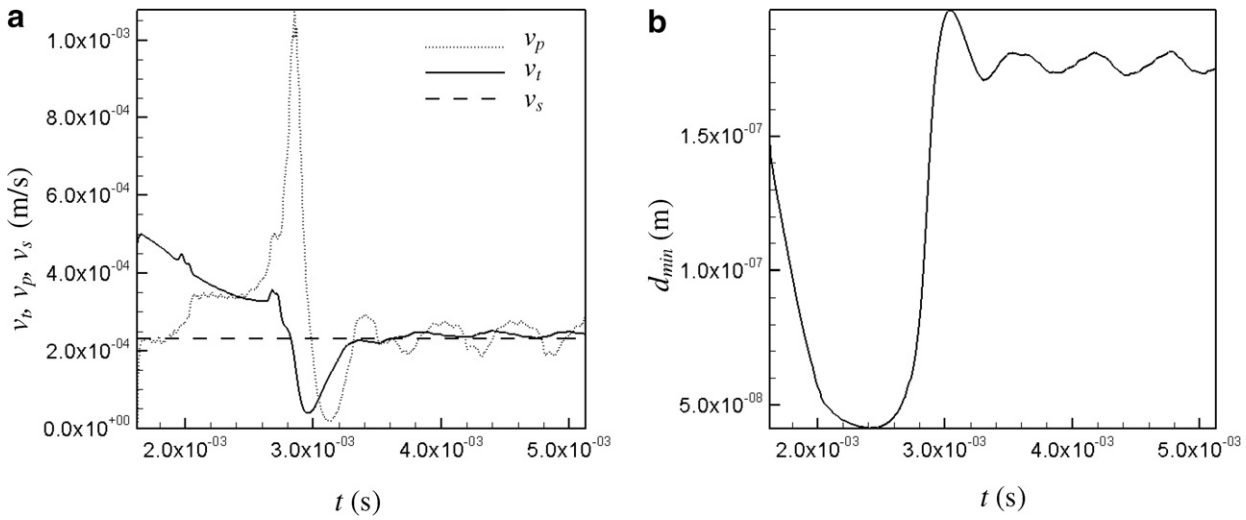

Fig. 9. Behavior of the particle for a solidification velocity = 230 μm/s, $\lambda = 2 \times 10^{-10}$ m (premelting included), $k_p/k_l = 0.01$, $R_p = 1$ μm. (a) Velocity versus time, the velocities of the particle (v_p), tip of the solidification front (v_t is the velocity of the front right under the particle) and the flat front away from the particle (v_s) are indicated in the figure. (b) d_{min} versus time, (c) drag (F_D) and repulsive intermolecular (F_I) force versus time and (d) the total force (F_T) versus time.

addition, the maximum in the curves (Fig. 10) found in the current study does not indicate a critical velocity. Instead, it simply indicates that the particle velocity has reached a maximum value and from that point in time the drag force increases and the particle will eventually be engulfed. However, engulfment does begin once the system has evolved to the left-hand side of the maximum (i.e. the particle begins to slow down as the d_{min} gets smaller).

It is noted that in the Rempel and Worster [6] work, only a $k_p/k_l = 1.0$ system was studied. However, in the case of metal-matrix composites, the ceramic particles are far less conductive than the metallic matrix, i.e. $k_p/k_l \ll 1$. In this case, as discussed above, pushing of the particles can result provided the solidification front velocity is lower than a critical value. The phase–space picture for $k_p/k_l = 0.01$ is shown in Fig. 10(b) for $v_s = 245$ μm/s. Note that the curves in Fig. 10(b) are very similar to the curves in Fig. 10(a), i.e. for this range of solidification velocities the particle is engulfed by the front. Fig. 10(c) shows the situation where the pushing to engulfment transition just occurs for the system under consideration. In the phase–plane plot in Fig. 10(c) it is seen that for $v_s = 245$ μm/s the evolution of the trajectory corresponds to the one for engulfment. However, for the 230 μm/s case the trajectory gets to a point near the maximum of the other curves but then deviates abruptly away to achieve a significantly higher velocity and large gap thickness d_{min}. Eventually the system settles as the velocity falls off and the gap thickness increases moderately. It appears as if the trajectory is drawn to an attractor in phase–space that corresponds to a quasi-steady pushing mode. This attractor is located at $v_p = v_t = v_s$. To establish a trend Fig. 10(d) shows the trajectory of a 220 μm/s solidification velocity case along with the previous 230 μm/s case. Somewhat surprisingly there is actually little difference in the final state for these two cases, i.e. the attractor is fairly stable to perturbations in the operating conditions. The one noticeable difference is that for the 220 μm/s case the trajectory does not approach the 'maximum' location of the engulfment cases (as is the case for the 230 μm/s trajectory) before it deviates towards the attractor at $v_p = v_s$. The deviation occurs very early in the evolution of the system for the lower velocity of 220 μm/s. These behaviors in the phase plane indicate strongly that the pushing–engulfment transition is a bifurcation in the evolution of the front-particle dynamical system and is induced by the competition between two attractors, one residing at the origin and the other at the $v_p = v_s$ value. The position of this attractor appears to be fairly stable to perturbations in the solidification velocity v_s. The location of this attractor may however depend on several parameters, such as the size of the particle, particle thermal conductivity and solid–liquid interfacial tension, and therefore a detailed parametric study is necessary to identify the critical velocity for a general system. Such a parametric study is currently being performed.

The insights obtained from the present study with regard to the determination of critical velocity for particle engulfment can be summarized as follows. Depending on the solidification parameters and conditions, the trajectory of the front-particle dynamical system in phase space can evolve towards one of two attractors, corresponding to the steady pushing or engulfment state. The cases above suggest that the fate of the particle is determined to a great extent by the curvature of the solidification front directly under the particle (in particular whether it becomes concave under it). Once the solidification front assumes a concave shape under the particle, whether due to thermal conductivity differences between the particle and melt or due to premelted film effects, engulfment becomes

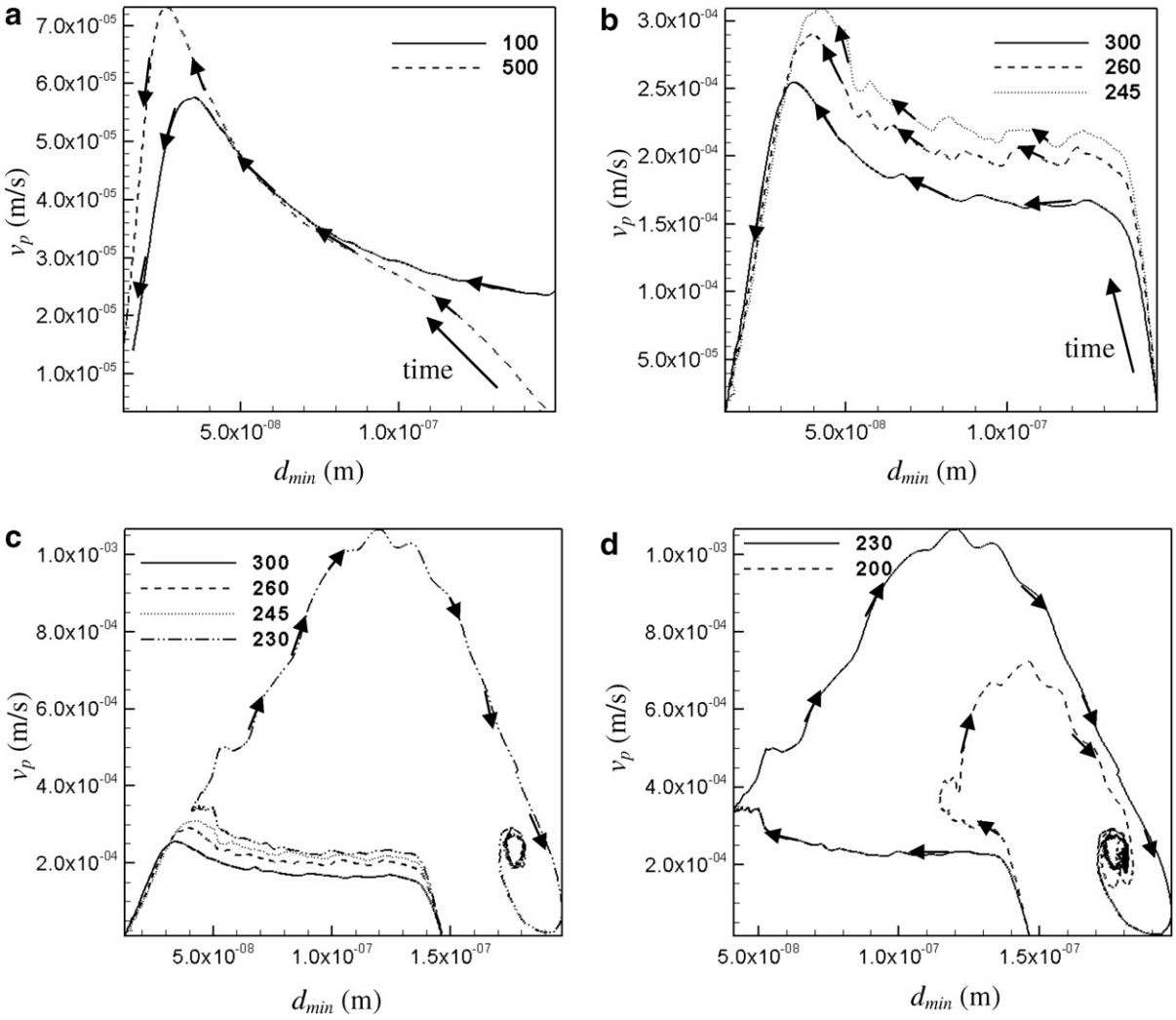

Fig. 10. (a) Phase–space plots for $k_p/k_l = 1.0$ at solidification (pull) velocities of 100 and 500 μm/s. The curves corresponding to each value of velocity are indicated in the legend. (b) Phase–space plots for $k_p/k_l = 0.01$ at solidification (pull) velocities of 245, 260 and 300 μm/s (see legend). Notice that these plots are very similar to Rempel and Worster [6]. These are all engulfment cases. (c) Phase–space plots for $k_p/k_l = 0.01$ at solidification (pull) velocities of 230, 245, 260 and 300 μm/s (see legend). The 230 μm/s case is the only pushing case – notice the large deviation from the engulfment cases suggesting a very sensitive non-linear process with two "attractors" in phase–space. (d) Phase–space plots for $k_p/k_l = 0.01$ at solidification (pull) velocities of 230 and 220 μm/s (see legend).

inevitable. However, if the solidification front is slow enough so that the bending of the front (i.e. the trend towards concavity) due to premelting does not overcome the convex protuberance of the front, the particle will travel along a completely different trajectory in phase–space and will be pushed by the front.

3. Conclusions

A multiscale method that was developed in Part I is employed to compute the interaction between a particle and a solidification front. The method allows one to capture arbitrary shapes and velocities of the different surfaces. The model computes the forces acting on the particle and moves the particle accordingly. From the computations, several conclusions were made about the nature of particle–solidification front interactions.

It was determined that at or near the critical velocity the system is quite sensitive to perturbations either causing engulfment or a significant deviation from the engulfment regime to a completely different path in phase–space – which indicates pushing. This is due to the complex interplay between the interface shape (due to k_p/k_l and premelting effects), the intermolecular repulsive forces (due to disjoining pressure) and drag forces (due to fluid motion). A particle being approached by a solidification front of a pure material that is directionally solidified will become engulfed when $k_p/k_l \geqslant 1.0$ as long as a premelted layer is assumed to exist between the particle and the front. This is due to the trough that forms underneath the particle and causes the large viscous drag to dominate and, hence, promote engulfment.

Insights into the mechanisms that determine the critical velocity (for $k_p/k_l < 1.0$) are obtained. The fate of the

particle is determined to a great extent by the curvature of the solidification front directly under the particle (i.e. whether it becomes concave or stays convex). Once the front assumes a concave shape under the particle, whether due to thermal conductivity differences between the particle and melt or due to premelted film effects, engulfment becomes inevitable. However, if the solidification front is slow enough so that the bending of the front (i.e. the trend towards concavity) due to premelting does not overcome the convex bump (for $k_p/k_l < 1.0$) of the front, the particle will travel along a completely different trajectory in phase–space and will be pushed steadily by the front.

Acknowledgement

This work was supported by a NSF-CAREER award (CTS-0092750) to the third author.

References

[1] D.R. Uhlmann, B. Chalmers, K.A. Jackson, Interaction between particles and a solid–liquid interface, J. Appl. Phys. 35 (1964) 2986–2993.
[2] J.N. Israelachvili, Intermolecular and Surface Forces, second ed., Academic Press, 1991.
[3] R. Asthana, S.N. Tewari, Second phase particle–solidification front interactions: an evaluation of theoretical models, Process. Adv. Mater. 3 (1993) 163–180.
[4] R. Asthana, S.N. Tewari, Review the engulfment of foreign particles by a freezing interface, J. Mater. Sci. 28 (1993) 5414–5425.
[5] J.G. Dash, H. Fu, J.S. Wettlaufer, The premelting of ice and its environmental consequences, Rep. Prof. Phys. 58 (1995) 115–167.
[6] A.W. Rempel, M.G. Worster, The interaction between a particle and an advancing solidification front, J. Cryst. Growth 205 (1999) 427–440.
[7] D.K. Shangguan, S. Ahuja, D.M. Stefanescu, An analytical model for the interaction between an insoluble particle and an advancing solid/liquid interface, Metal. Mater. Trans. A 23A (1992) 669–680.
[8] A.V. Catalina, S. Mukherjee, D.M. Stefanescu, A dynamic model for the interaction between a solid particle and an advancing solid/liquid interface, Metal. Mater. Trans. A 31A (2000) 2559–2568.
[9] J.W. Garvin, H.S. Udaykumar, Particle–solidification front dynamics using a fully coupled approach. Part I: Methodology, J. Cryst. Growth 252 (2003) 451–466.
[10] J.W. Garvin, H.S. Udaykumar, Particle–solidification front dynamics using a fully coupled approach. Part II: Comparison of drag expressions, J. Cryst. Growth 252 (2003) 467–479.
[11] G.F. Bolling, J. Cisse, A theory for the interaction of particles with a solidifying front, J. Cryst. Growth 10 (1971) 56–66.
[12] J.W. Garvin, H.S. Udaykumar, Effect of a premelted film on the dynamics of particle–solidification front interactions, J. Cryst. Growth 290 (2) (2006) 602–614.
[13] L. Hadji, Thermal force induced by the presence of a particle near a solidifying interface, Phys. Rev. E 64 (51) (2001) 51502/1–51502/6.
[14] D.M. Stefanescu et al., Particle engulfment and pushing by solidifying interfaces: Part II. Microgravity experiments and theoretical analysis, Metal. Mater. Trans. A 29A (1998) 1697–1706.
[15] A.M. Zubko, V.G. Lobanov, V.V. Nikonova, Reaction of foreign particles with a crystallization front, Sov. Phys. Crystallogr. 18 (2) (1973) 239–241.
[16] A.A. Chernov, D.E. Temkin, A.M. Mel'nikova, Theory of the capture of solid inclusions during the growth of crystals from the melt, Sov. Phys. Crystallogr. 21 (4) (1976) 369–373.
[17] A.A. Chernov, D.E. Temkin, A.M. Mel'nikova, The influence of the thermal conductivity of a macroparticle on its capture by a crystal growing from a melt, Sov. Phys. Crystallogr. 22 (6) (1977) 656–658.
[18] A. Borsik, K.K. Kelemen, G. Kaptay, A dynamic model of ceramic particle–solidification front interaction, Mater. Sci. Forum 414–415 (2003) 371–376.